China Geology 6 (2023) 429–442

China Geology

Journal homepage: http://chinageology.cgs.cn
https://www.sciencedirect.com/journal/china-geology

Tectonic-thermal history and hydrocarbon potential of the Pearl River Mouth Basin, northern South China Sea: Insights from borehole apatite fission-track thermochronology

Xiao-yin Tang[a, b, c,*], Shu-chun Yang[d], Sheng-biao Hu[e]

[a] *Institute of Geomechanics*, *Chinese Academy of Geological Sciences*, *Beijing* 100081, *China*
[b] *Key Laboratory of Petroleum Geomechanics*, *China Geological Survey*, *Beijing* 100081, *China*
[c] *Key Laboratory of Paleomagnetism and Tectonic Reconstruction*, *Ministry of Natural Resources*, *Beijing* 100081, *China*
[d] *CNOOC Research Institute*, *Beijing* 100028, *China*
[e] *State Key Laboratory of Lithospheric Evolution*, *Institute of Geology and Geophysics*, *Chinese Academy of Sciences*, *Beijing* 100029, *China*

ARTICLE INFO

Article history:
Received 17 March 2022
Received in revised form 25 July 2022
Accepted 25 August 2022
Available online 20 September 2022

Keywords:
Oil and gas
Hydrocarbon potential
Apatite fission-track
Tectonic-thermal evolution
Thermal history modeling
Cooling event
Heating event
Marine geological survey engineering
Erosion amount and rate
Oil-gas exploration engineering
Pearl River Mouth Basin
The South China Sea

ABSTRACT

The Pearl River Mouth Basin (PRMB) is one of the most petroliferous basins on the northern margin of the South China Sea. Knowledge of the thermal history of the PRMB is significant for understanding its tectonic evolution and for unraveling its poorly studied source-rock maturation history. Our investigations in this study are based on apatite fission-track (AFT) thermochronology analysis of 12 cutting samples from 4 boreholes. Both AFT ages and length data suggested that the PRMB has experienced quite complicated thermal evolution. Thermal history modeling results unraveled four successive events of heating separated by three stages of cooling since the early Middle Eocene. The cooling events occurred approximately in the Late Eocene, early Oligocene, and the Late Miocene, possibly attributed to the Zhuqiong II Event, Nanhai Event, and Dongsha Event, respectively. The erosion amount during the first cooling stage is roughly estimated to be about 455–712 m, with an erosion rate of 0.08–0.12 mm/a. The second erosion-driven cooling is stronger than the first one, with an erosion amount of about 747–814 m and an erosion rate between about 0.13–0.21 mm/a. The erosion amount calculated related to the third cooling event varies from 800 m to 3419 m, which is speculative due to the possible influence of the magmatic activity.

1. Introduction

The exploration and production from deepwater reservoirs globally have been increased to meet the growing demand for oil and gas. Explorations have been focused on the deepwater to ultra-deepwater passive margins, especially the base of the slope or the continent-ocean boundary area (White N et al., 2003). The Pearl River Mouth Basin (PRMB) is one of the most important oil & gas-bearing basins located on the northern margin of the South China Sea (SCS), thus has attracted the interest of numerous researchers and oil exploration companies, especially after the finding of a series of commercial discoveries in its deep-water areas (Zhu WL et al., 2012). Distinguishing from basins on many other passive margins, the PRMB on the northern SCS margin is characterized by multi-episodic rifting stages and corresponding heating events (He LJ et al., 2001; Song Y et al., 2011), active tectonic events during the post-rifting phase, such as abnormal thermal subsidence (Clift P and Lin J, 2001; Xie XN et al., 2006; Tang XY et al., 2017), and magmatism (Li ST et al., 1999; Yan P et al., 2006), relatively high heat flow continues until now (Shi XB et al., 2003; Tang XY et al., 2014). The episodes of rifting and heating would be conducive to the overprinted structures development and the deposition of several discrete transgressive packages of source rocks and reservoirs. The thermal maturity of sedimentary organic matter affected by multi-episodic rifting and subsidence would be higher than expected on a typical passive margin of equivalent age that had not experienced repeated heating (Ru K et al., 1994). It is indeed because of the

* Corresponding author: *E-mail address*: xytang2019@126.com (Xiao-yin Tang).

Literary editor: Xi-jie Chen
doi:10.31035/cg2022055
2096-5192/© 2023 China Geology Editorial Office.

complex tectonic evolution since the Late Mesozoic, that the PRMB experienced relatively complex thermal history evolution that was very difficult to be unraveled.

The thermal history of sedimentary basins has garnered increasing interest in basin analysis because it is closely related to the deep geodynamic mechanism (Rudnick RL et al., 1998; Qiu NS et al., 2014), oil and gas accumulation, and petroleum resource evaluation (Carminati E et al., 2010; Qiu NS et al., 2012; Zuo YH et al., 2017). Unfortunately, the research on the thermal history of the PRMB is currently in its infancy and hampered by the boreholes and data availability due to the high cost of offshore drilling. Several campaigns have been carried out, mainly focusing on the heat flow evolution of the PRMB using mathematical models based on a seismic and stratigraphic framework (Song Y et al., 2011; Tang XY et al., 2018a; 2018b; Li YJ et al., 2019). Although those achievements have shed light on the basic paleo heat flow evolution of the PRMB, detailed information on the tectonic-thermal evolution of the PRMB, such as the maximum burial temperature, the erosion thickness has not been well studied so far. Apatite fission-track (AFT) thermochronology, which is sensitive to temperatures of 60°C–120°C (partial annealing zone or PAZ (Gleadow A et al., 1986)), has been widely used to investigate geological problems including the thermal history reconstruction of sedimentary basins (Gallagher K et al., 1998; Kohn BP et al., 2005; Xiang CF et al., 2013; Tian ZH et al., 2016; Zhang ZY et al., 2016; Tang XY et al., 2019; Jiang S et al., 2021).

Here, this paper presents new AFT analyses of 12 samples from 4 boreholes in the PRMB. These results, combined with the thermal history modeling, reveal a complex Middle Eocene–Recent thermal evolution. Besides contributing to understanding the tectonic-thermal history scenario of the PRMB, this study allowed the rate and thickness of the erosion events to be determined. Notably, this work presents the results of AFT dating from samples submerged in deep-water northern SCS. The dating of such samples provides information for constraining the deformation time in hardly accessible areas.

2. Geologic setting and present geothermal region

The continental margin along with northern SCS, located at the junction of the Indo-Australian Pacific, and Eurasian Plates, experienced widespread deformation since the Mesozoic (Li XJ et al., 2022; Ye Q et al., 2018). Situated on the northern margin of the SCS, the NE-trending PRMB contains mainly five structural units, that is from north to south, the Northern Uplift Zone, the Northern Depression (Zhu I and Zhu III Depressions), the Central Uplift Zone (Shenhu Uplift, Panyu Low-uplift, and Dongsha Uplift), the Southern Depression Zone (Zhu II and Chaoshan Depressions), and the Southern Uplift Zone (Fig. 1).

Fig. 2 presents the stratigraphy for the PRMB. The Tg, T90, T80, T70, and T20 unconformities are sequence boundaries related to the Shenhu, Zhuqiong I, Zhuqiong II, Nanhai, and Dongsha Events or “Movements”. The evolution of the PRMB is complex and can be generally divided into syn-rift and post-rift stages (Zhou D et al., 1995). Although the timing of rifting termination is still ambiguous (Clift and Lin, 2001; Dong DD et al., 2008; 2009; Tang XY et al., 2018a; 2018b; Wang PC et al., 2020), the T70 unconformity, at the base of the Zhuhai Formation, was considered as the boundary of syn-rift and post-rift strata (Xie H et al., 2013). The syn-rift sediments consist of the Paleocene-Early Eocene Shenhu, Middle Eocene Wenchang, and Late Eocene Enping Formations. The Shenhu Formation mainly consists of alluvial fan sands and conglomerates associated with volcanic sediments. Sediments in this Formation are absent across much of the PRMB. Deposited in a deep- to shallow-water lacustrine environment, the Wenchang Formation is mainly composed of grey to black mudstones and sandstones. The Enping Formation was deposited in a shallower-water lacustrine setting, comprising grey to black mudstones with interbedded sandstones and coal seams (Zhu WL et al., 2009). The coals and mudstones in the Wenchang and Enping Formations are major source rocks of oil and gas in the PRMB (Zhu WL et al., 1999). During the post-rift stage, the Oligocene Zhuhai, Early Miocene Zhujiang, Middle Miocene Hanjiang, Late Miocene Yuehai, Pliocene Wanshan Formations, and Quaternary series were deposited, comprising transitional deltaic, shelf to abyssal marine sediments.

The PRMB presents the characteristics of a typical “hot” basin (Rao CT and Li PL, 1991; He LJ et al., 2001; Yuan YS et al., 2009; Tang XY et al., 2014; 2016). The geothermal gradient varies from 24.7 °C/km to 60.8 °C/km, with an average value of 37.9±7.4 °C/km. Heat flow ranges from 24.2 mW/m^2 to 121.0 mW/m^2, with an average value of 71.8±13.6 mW/m^2. Generally, the geothermal gradient and heat flow values increase from the shelf in the north to the continental ocean boundary in the south.

3. Samples and methodology

We collected 12 cutting samples of four boreholes in the PRMB (locations see Fig. 1). Sample details are presented in Table 1.

Apatite grains were separated by the standard heavy mineral separation techniques in the Institute of Regional Geology and Mineral Resources, Hebei Province, China. Fission-track analyses were performed at Apatite to Zircon, Inc. (A to Z). Apatite grain-mount preparation details were presented in Donelick RA et al. (2005). After polishing, sample mounts were etched in 5.5 M HNO_3 for 20.0 s (± 0.5 s) at 21°C (±1°C) to reveal the spontaneous fission tracks. Fission-track was viewed, counted, and measured at 1562.5× dry magnification using unpolarized transmitted light and a Nikon Optiphot2 microscope. Apatite fission-track ages were obtained using direct measurements of uranium concentrations with LA-ICP-MS. The uranium concentration of each counted grain was determined through 26 μm spot

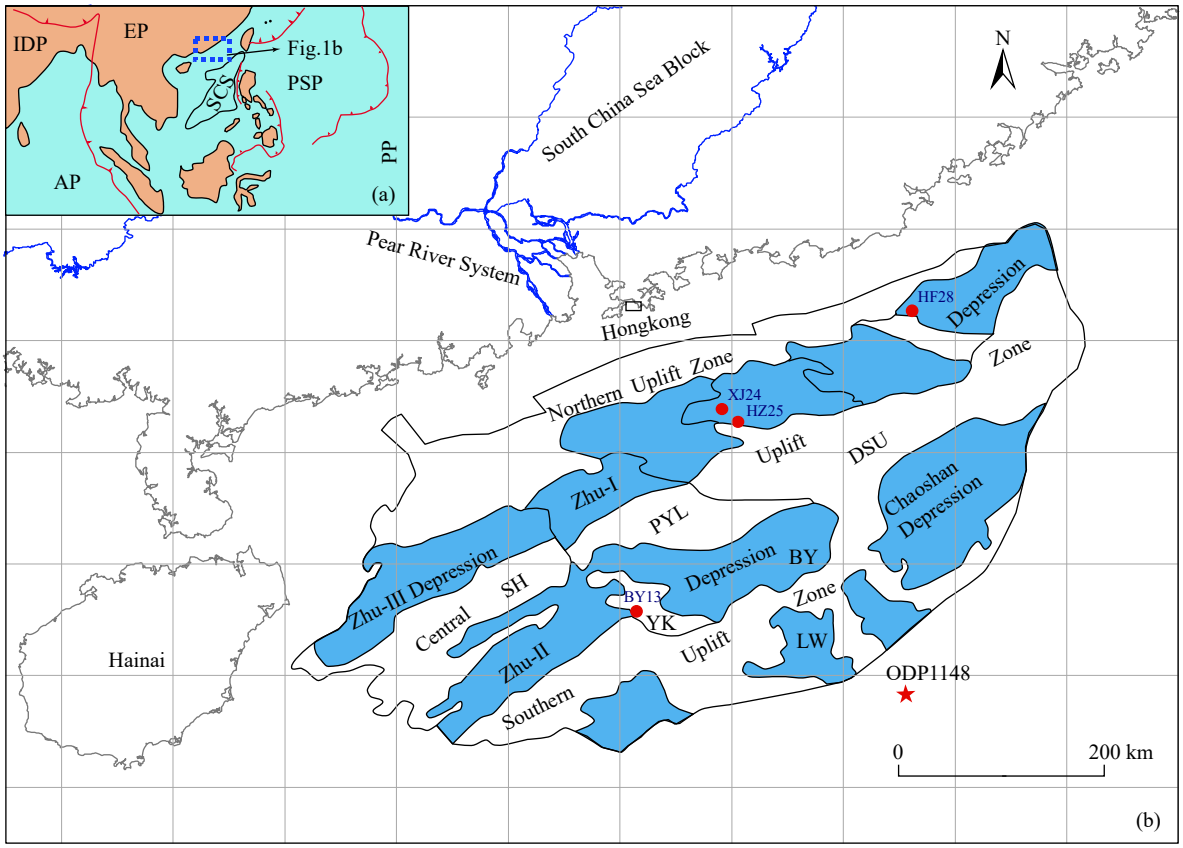

Fig. 1. Map showing the Pearl River Mouth Basin in a regional context (a) and the subdivision of this basin (b). EP–Eurasian Plate, IDP–India Plate, SCS–South China Sea, PSP–Philippine Sea Plate, PP–Pacific Plate, AP–Australian Plate. SH–Shenhu Uplift, PYL–Panyu Low-uplift, DSU–Dongsha Uplift, YK–Yunkai Low-uplift, BY–Baiyun Sag, LW–Liwan Sag. Red circles in (b) show the sample wells in this work and the red star presents the location of the ODP Site 1148.

analyses using an Agilent 7700x Quadrupole ICP-MS, coupled to a Resonetics M-50 193 nm ArF Eximer laser-ablation system following analytical settings as described in Donelick RA et al. (2005). Fission-track ages were calculated following the scheme proposed by Donelick RA et al. (2005). AFT lengths were measured on horizontal confined fission tracks.

Usually, the grain-age distribution is subjected to a χ^2 test to assess the homogeneity of AFT ages (Galbraith RF, 1990). Chi-square (P (χ^2)) value over 5% means that there is a > 95% chance that the dated sample has a single population, while P (χ^2) < 5% is diagnostic of multiple populations.

4. Results and interpretation

AFT ages and confined track length measurements are shown in Table 2, the raw dataset is presented in the Supplementary tables (Tables. S1–S12). 6 of 12 of the samples failed the χ^2 test, indicating considerable age dispersion. To approximate distinct age populations, we employed RadialPlotter (Vermeesch P, 2009) to get multicomponent age data which are presented in Fig. 3. In the plot of age vs depth/present temperature (Fig. 4), pooled ages were presented if samples pass the χ^2 test, otherwise, central ages were presented.

In Well BY13, samples at depths of 1698 m and 1785 m in the Zhuhai Formation (BY131) and Enping Formation (BY132) failed the χ^2 test (Table 2). AFT central ages are 43.8±3.4 and 42.2±3.9 Ma, respectively, older than their stratigraphic ages (Table 2, Fig. 4a). Sample from the Wenchang Formation (BY133) at a depth of 1907 m passed the χ^2 test (P (χ^2) = 22%). The pooled age is 52.7±2.4 Ma, slightly larger than its stratigraphic age (Table 2, Fig. 4a). All the three central or/and pooled ages are older than the stratigraphic age, suggesting that they have not undergone fully post-depositional annealing. However, the partial post-depositional annealing is evident from the considerable dispersion in single grain ages with part of grains showing AFT ages younger than the stratigraphic age. The confined track lengths vary from 7.5 μm to 15.0 μm in sample BY131, 10.9 μm to 15.8 μm in sample BY132, and 7.1 μm to 15.9μm in sample BY133 (Tables. S1–S3, Figs. S1(a)–(c)). The large dispersion in single grain ages and track lengths distribution may attribute to annealing kinetic parameters (e.g. D_{par}, Cl content) (Donelick RA et al., 2005), variations in source regions with different exhumation histories, and/or rather complicated thermal history. Possibly because of the limited confined track numbers, there is no clear relationship presented in the plot of confined track lengths *vs* D_{par} (Fig. S2). Although very weak, it seems to show a positive relationship between age and the D_{par} value of most of the 12 samples (Fig. S3).

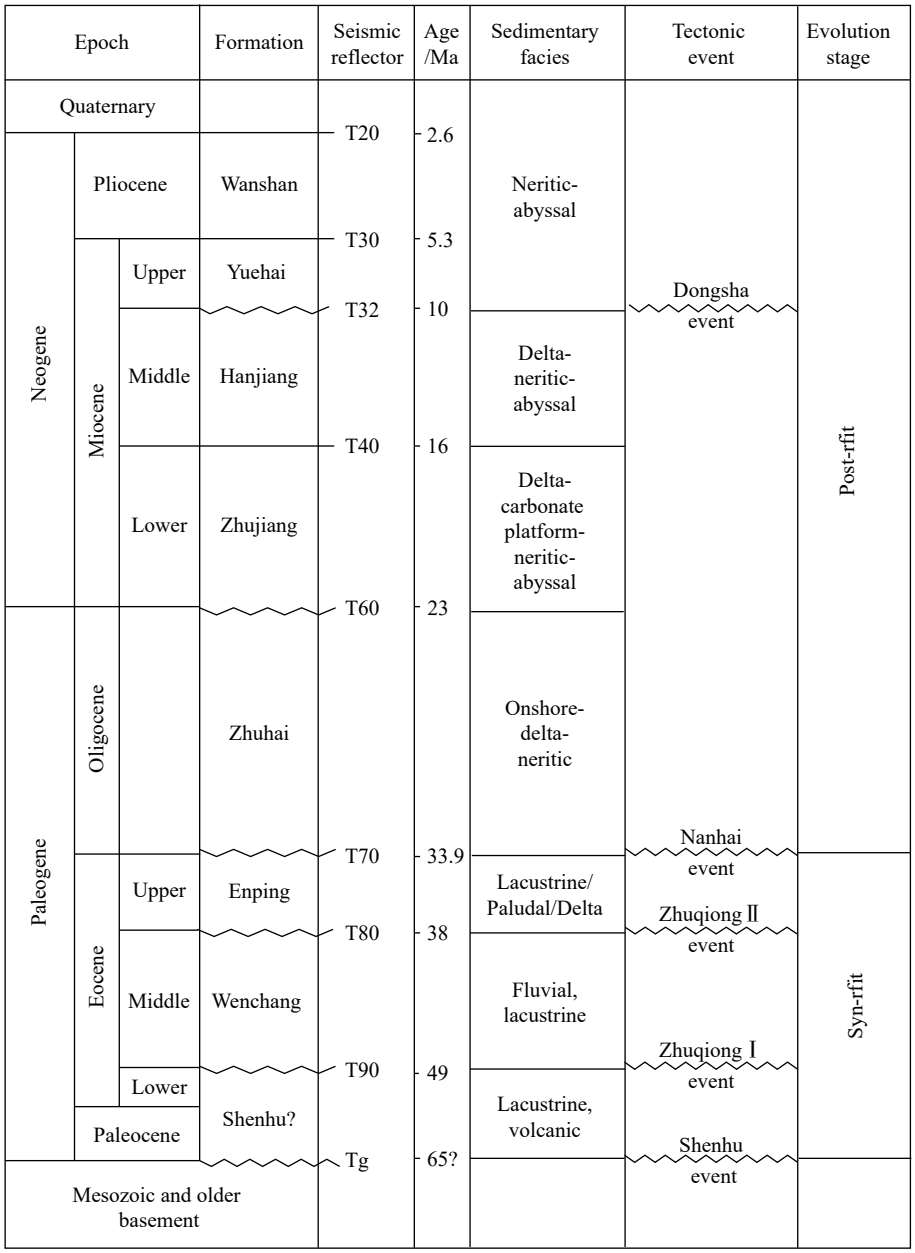

Fig. 2. Generalized stratigraphic column of the Pearl River Mouth Basin showing main seismic reflectors, depositional facies, and tectonic events (after Tang XY et al., 2017).

In Well XJ24, sample XJ241 from the uppermost Zhuhai Formation at depth of 3141 m failed the χ^2 test. Although the central age of 8.9±1.9 Ma is younger than its stratigraphic age, the single grain ages of sample XJ241 show a large range with a dispersion value of 70%, and some grain ages younger than the stratigraphic age (Table 2, Fig. 4b). These characteristics indicate that sample XJ241 experienced at least partial annealing. Sample XJ242 at depth of 3770 m from the Enping Formation passed the χ^2 test (P (χ^2) = 24%), with a pooled age of 10.4±2.9 Ma. All the single-grain ages of sample XJ242 are younger than its stratigraphic age, which may indicate that the sample passed the PAZ at about 10.4 Ma. At depth of 3985 m, sample XJ243 from the Wenchang Formation presents a pooled age of 2.2±0.8 Ma. Most of its single grain ages are about 0 Ma, indicating nearly complete annealing. Importantly, the present temperature at the sample depth is very high (116°C–142°C) (Table 1, Fig. 4b), which theoretically totally erases all existing spontaneous fission tracks in common apatite grains. However, the AFT results indicate that the fossil fission tracks in apatite samples could have survived under such temperature conditions, therefore suggesting probably very recent heating and/or high D_{par} value. This interpretation is also consistently supported by the preserved confine tracks, with a mean length of 10.1±1.0 μm.

In the well HZ25, a limited number of grain ages and confined tracks have been analyzed due to the sample quality and high present temperature (134°C–153°C). Sample HZ251 from the Zhuhai Formation and sample HZ253 from Wenchang Formation passed the χ^2 test and presented pooled ages of 6.4±3.2 and 4.8±3.4 Ma (Table 2). Sample HZ252 from the Enping Formation failed the χ^2 test (P (χ^2) = 0) and yielded a central age of 18.0±10.0 Ma. Although few grain

Table 1. Basic information of samples used in this study.

Sample	WD/m	ST/°C	G/(°C/km)	D/mb.s.	PT/°C	Fm.	Stratigraphic age/Ma	Lithology
BY13	688[a]	6.8[a]	45.9[a]					
BY131				1698	85	Zhuhai	23–33.9	sandstone
BY132				1785	89	Enping	33.9–38	coarse sandstone
BY133				1907	94	Wenchang	38–49	medium sandstone
XJ24	100[a]	22.0[a]	30[c]					
XJ241				3141	116	Zhuhai	23–33.9	sandstone
XJ242				3770	135	Enping	33.9–38	sandstone, siltstone
XJ243				3985	142	Wenchang	38–49	sandstone, conglomerate
HZ25	104[a]	21.8[a]	35.5[b]					
HZ251				3149	134	Zhuhai	23–33.9	sandstone
HZ252				3322	140	Enping	33.9–38	sandstone
HZ253				3706	153	Wenchang	38–49	sandstone
HF28	51[a]	24.2[a]	28.1[c]					
HF281				2039	81	Zhuhai	23–33.9	fine sandstone
HF282				2243	87	Enping	33.9–38	fine, medium sandstone
HF283				3171	113	Wenchang	38–49	coarse, medium sandstone

WD–water depth; ST–seafloor temperature; G–Geothermal gradient; D (m b.s.) –Depth in meter below seafloor; PT –present temperature, PT=ST+G*D/1000. [a] is from CNOOC. [b] is from Tang XY et al. (2014). [c] is from Rao CT and Li PL (1991).

Table 2. Apatite fission-track data from the Pearl River Mouth Basin, northern South China Sea.

Sample	Age										Length		
	N	*N*s	D_{par} /μm	Pooled age /Ma	1σ	Central age/Ma	1σ	P(χ^2)/%	D/%	Tracks	MCT/ μm	Std/μm	Dpar/μm
BY13													
BY131	36	493	1.9	45.2	2.3	43.8	3.4	0.0	29	174	12.2	1.4	2.1
BY132	34	291	2.0	42.8	2.6	42.2	3.9	0.0	33	175	12.4	1.4	2.3
BY133	33	564	2.0	52.7	2.4	53.7	2.8	22.0	12	187	12.0	1.5	2.3
XJ24													
XJ241	29	112	1.7	8.2	0.8	8.9	1.9	0.0	70	51	11.2	1.4	2.3
XJ242	7	13	1.9	10.4	2.9	12.9	4.3	24.0	34	4	11.6	0.4	2.2
XJ243	16	8	1.9	2.2	0.8	3.8	1.4	88.0	23	8	10.6	1.0	2.1
HZ25													
HZ251	3	4	1.8	6.4	3.2	8.2	4.1	35.0	0	1	14.1	0.0	2.6
HZ252	9	10	2.0	4.8	1.5	18.0	10.0	0.0	113	2	15.4	0.9	2.7
HZ253	6	2	2.2	4.8	3.4	20.0	14.0	100.0	0	2	14.9	1.2	2.8
HF28													
HF281	18	123	1.9	46.6	4.4	48.9	7.1	1.0	39	61	11.6	1.3	2.2
HF282	7	25	2.1	42.4	8.6	47.0	10.0	55.0	14	10	11.4	1.3	2.3
HF283	32	77	2.0	15.1	1.8	43.0	11.0	0.0	117	17	11.3	1.1	2.6

N and *N*s are the numbers of grains and spontaneous tracks; MCT–mean confined track length; Std–standard deviation

ages from sample HZ252 are older than the corresponding stratigraphic age, most of the grain ages are about 0 Ma (Table S8; Fig. 4c). Given the remarkably high present temperature of 134°C–153°C, a total reset of fossil tracks in the apatite grains would be expected to occur. However, the apatite samples still contain a long track component, for example, confined track length up to 16.1 μm for sample HZ253 at the bury temperature of 153°C. It is suggested that samples might have recently been subjected to high temperatures and/or high D_{par} value (D_{par}=2.81 μm).

In the Well HF28, only the sample from the Enping Formation (HF282) at depth of 2039 m fulfilled the χ^2 test (P(χ^2) = 55%) (Table 2). Pooled age of sample HF282 is 42.4±8.6 Ma, while the central age of samples HF281 and HF283 is 48.9±7.1 Ma and 43.0±11.0 Ma, respectively. All three samples present part of single-grain ages younger than their stratigraphic age (Fig. 4d), pointing to partial thermal overprint. The mean confined track lengths vary from 11.3±1.1 μm (sample HF283) to 11.6±1.3 μm (sample HF281) (Table 2). The spread range of the length distribution (Figs. S1(j)-(l)) suggests that the samples have experienced quite complex thermal history.

5. Thermal history reconstruction

A quantitative evaluation of thermal history can be obtained through the application of statistical modeling procedures that find time-temperature paths (t-T) compatible with the fission-track data (grain ages plus length

distributions) (Gallagher K, 1995; Ketcham RA, 2005). Seven samples (XJ241, HF281, HF282, HF283, BY131, BY132, BY133) with more than 10 measured confined fission-track lengths were chosen to reconstruct the thermal history by HeFTy (version 1.9.3) (Ketcham RA et al., 2018). This version allows the stratigraphic and pre-depositional relationships between a set of sample files from the same well to be established.

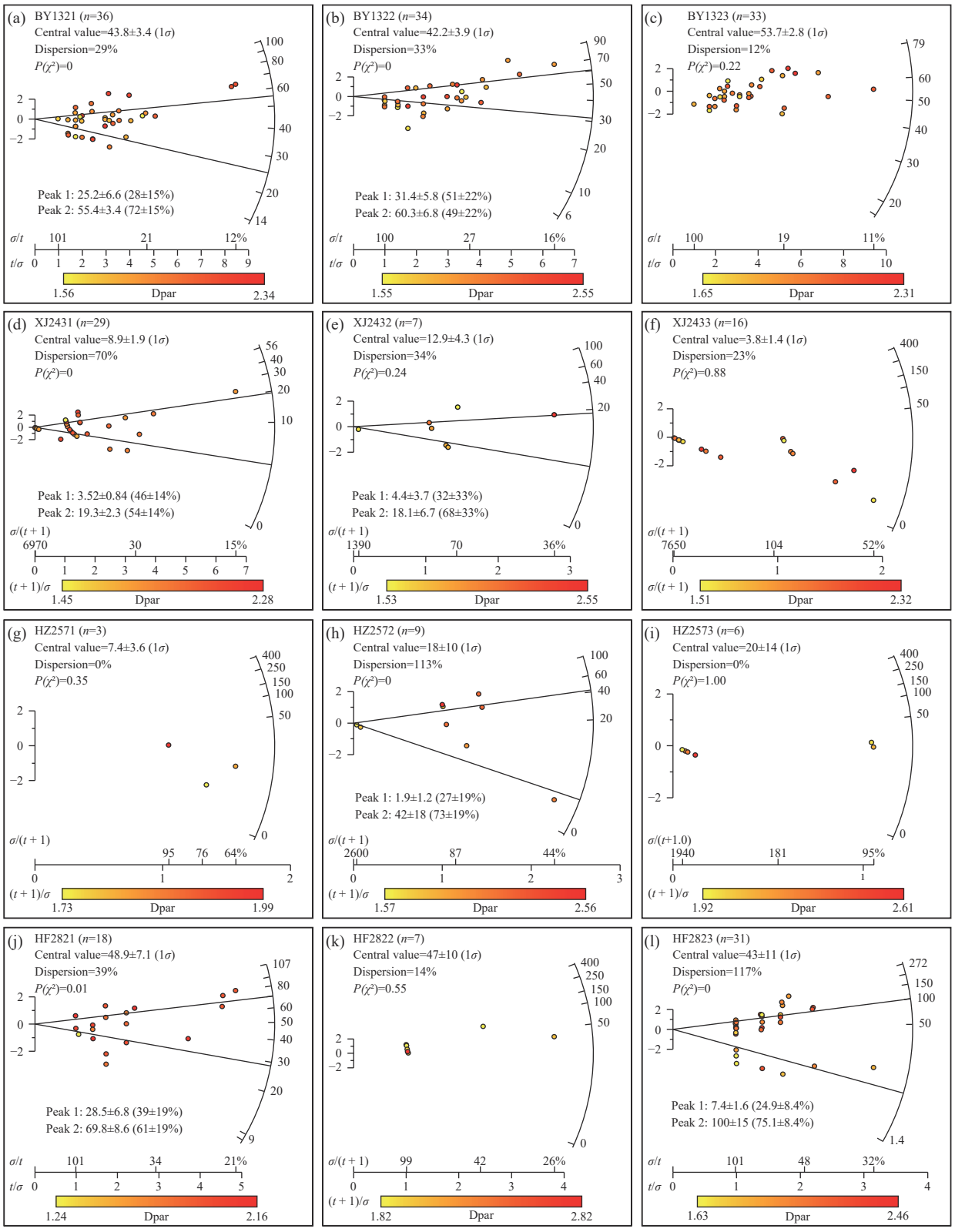

Fig. 3. Radial plots of apatite fission-track data. Single-grain ages are color-coded according to their D_{par}. *n*–number of analyses and dispersion gives the age-dispersion value as a percentage. Black lines represent statistically derived AFT population ages using the mixture model in RadialPlotter.

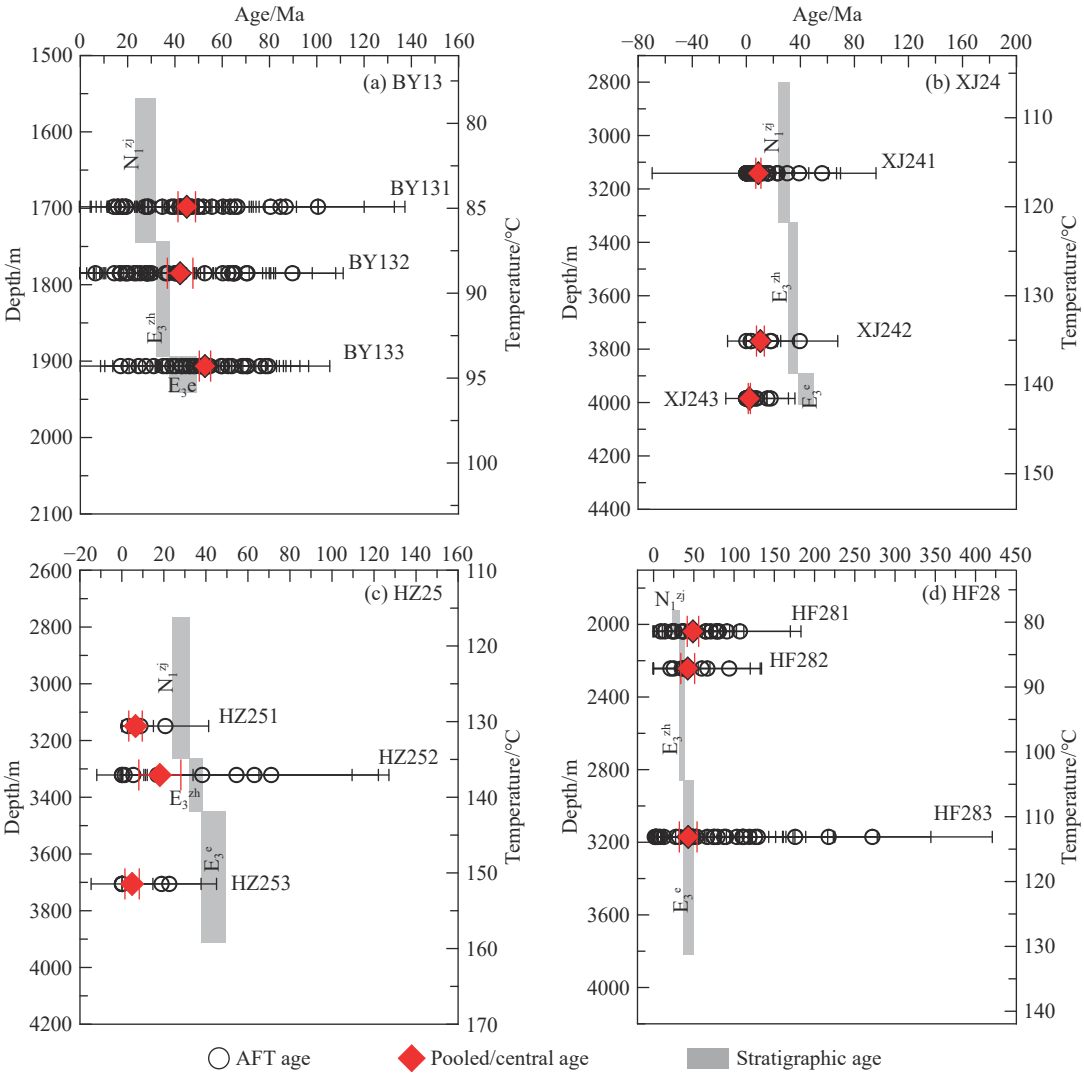

Fig. 4. Apatite fission-track single grain ages and pooled/central ages (±1σ) vs depth/present temperature distribution of the well (a) BY13, (b) XJ24, (c) HZ25, and (d) HF28. Pooled ages are presented when P (χ^2) > 5%, otherwise, the central ages are presented.

5.1. Data preparation

It is noteworthy that the pooled or/and central ages of the seven samples are geologically meaningless as they represent a mixture of ages both younger and older than the corresponding stratigraphic ages. To decipher the thermal history from the mixture ages, we separated the single-grain ages of samples that failed the χ^2 test into two populations concerning for D_{par} value and tried our best effort to seek groups that pass the χ^2 test. Separation details are presented in Table 3. For sample BY131, when c-axis projected track length data were used, the model produces only acceptable, but not good solutions. Thus, we used the non-projected data which could be well fitted. Due to the lack of good and acceptable fit results, only the older group age data of sample HF283 were incorporated into modeling in the well HF28.

5.2. Strategy and constraints on modeling

A primary goal of thermal history modeling is to test the plausible range of thermal history scenarios that can reproduce an observed data set. Modeling can be generated in either a forward or inverse sense. Here we follow a strategy that first uses a forward model-based approach, and then, a refined search of t-T space by inverse modeling. The inversion model in HeFTy uses a Monte Carlo method to test t-T paths that pass through certain, user-specified t-T constraint boxes. These boxes are implemented based on the geologic observations and used to test specific t-T hypotheses. Except for the AFT age and track length dataset obtained from this study, additional geological constraints were incorporated in the modeling, including: (1) the temperature at deposition time (assumed to be 15±10°C); (2) current temperature at the sample depth as presented in Table 1; (3) initial early constraint, consisting of initial cooling from above the closure temperature of AFT systems and at least 1.5 times earlier than the oldest age group (Ketcham RA, 2005); (4) uplift and erosion attributed to the Zhuqiong II, Nanhai, and Dongsha Events (Jiang ZL et al., 2012; Wu SG et al., 2014).

Keeping all the above constraints in mind, the modeling process was conducted with the forward approach firstly, then

Table 3. Thermochronometric data for thermal history modeling.

Sample	Population	D_{par}/ μm	N_{grains}	Age/ Ma	1σ	N_{tracks}	Lc mean/ μm	Std/ μm
BY13								
BY131	1	1.9	31	45[a]	2.4	119	13.36[c]	0.9
	2	2.6	5	47.4	7.2	55	13.41	1.0
BY132	1	1.9	30	42.8[a]	2.8	102	13.54	0.9
	2	2.6	4	43.4	8.3	73	13.63	1.1
BY133	1	2.2	33	52.7	2.4	187	13.25	1.0
XJ24								
XJ241	1	1.8	26	8.1[a]	0.8	3	12.50	0.2
	2	2.7	3	14.0	7.0	48	12.63	0.9
HF28								
HF281	1	1.5	15	46.2[a]	4.5	10	12.77	1.1
	2	2.2	3	51.9	17.4	51	12.97	0.8
HF282	1	2.8	7	42.4	8.6	10	12.89	1.1
HF283	1	1.9	29	14.7[a, b]	1.8	9	12.57	0.5
	2	2.7	2	50.3	29.2	8	12.93	0.62

Population: AFT grains were split into two populations based on D_{par} value, with N_{grains} and N_{tracks} indicating the number of dated grains and track lengths in each population. Lc mean–mean track length after c-axis correction. [a] Population does not pass the chi-squared test. [b] Not used for inverse modeling. [c] For sample BY131, non-projected tracks were used.

the inverse modeling was performed based on the best forward model until 50 good fits were found.

5.3. Modeling results

Modeling results are presented in Figs. 5–7 as path envelopes. The uncertainty is presented in the plots in green and pink according to the reliability. As samples BY133 and HF283 are from the lowermost Wenchang Formation, they resented a relatively more complete thermal history than the other five samples. The following discussion sections are thus mainly based on the thermal history revealed by samples BY133 and HF283. Both of them show overall similar thermal histories that since the deposition of the Wenchang Formation, the PRMB underwent a very complex thermal history with seven distinct stages: (1) heating during about 45–41 Ma, (2) cooling during about 41–36 Ma, (3) heating during about 36–32 Ma, (4) cooing during 32–28 Ma, (5) heating during 28–13 Ma, (6) cooling during about 13–9 Ma, and (7) heating from about 9 Ma to present.

6. Discussions

6.1. Coupling relationship of thermal history with tectonic evolution

The weighted mean t-T paths of the thermal models were shown in Fig. 8a. As indicated by the modeling result, hinterland rock uplift and exhumation occurred approximately in the Late Cretaceous (about 70 Ma). Despite the provenance of the sediments in the PRMB is still controversial, the South China Block has long been viewed as the main source area (Shao L et al., 2016, 2017; Liu C et al., 2017; Wang W et al., 2017). Coincidentally, a cooling/exhumation phase from about 70 Ma onwards in the southern South China Block was also recorded by the AFT data (Yan Y et al., 2009). However, due to the partially reset of AFT ages, cooling history in the source area is poorly constrained and not discussed further in this study. Since the oldest sample is from the Wenchang Formation, we paid more attention to the thermal evolution since the early Middle Eocene.

From Paleocene to early Middle Eocene, there are two phases of rifting (corresponded with the Shenghu Event and Zhuqiong Zhuqiong I Event) due to the back-arc extension of the Pacific Plate subduction and the joint effect between the Indo-Eurasian collision and the Pacific Subduction domains, respectively (Wang PC et al., 2020, 2021). Multiples rifting resulted in the dominant northeast faults and faulting arrays defining a series of graben and half-grabens. Organic-rich mudstones were deposited in deep lakes; these mudstone beds formed the very important source of the Wenchang Formation (Zhang CM et al., 2004) (Fig. 2). After the deposition, the samples were subjected to heating to temperatures of about 41°C–61°C until about 41 Ma (Fig. 8a).

During the late Middle Eocene to Early Oligocene, the Pacific Plate subduction direction changed from NNW to WNW and the convergence rate slightly increased (Fig. 8c), resulting in the retreat of the Pacific subduction zone and the back-arc extension (Maruyam S and Send T, 1986; Northrup CJ et al., 1995). Simultaneously, the Indian Plate moved northeastwards with a gradually declining plate velocity (Fig. 8b) (Lee T and Lawver LA, 1995; Torsvik TH et al., 2008). At the same time, the southward subduction of the proto-SCS produced slab pull force in the continental margin of the South China Block (Fig. 8b; Wang PC et al., 2020, 2021). Therefore, under the joint effect of these three dynamic systems, the Zhuqiong Ⅱ Event occurred, leading to erosion and the third rifting (Wu XJ et al., 2009; Jiang ZL et al., 2012). During this period, samples underwent cooling between about 41–35 Ma and heating until about 32 Ma (Fig. 8a). In response to the seafloor spreading, the Nanhai Event happened in the early Oligocene, causing tectonic uplift and sediment erosion. Samples thus experienced cooling during about 32–27 Ma and reheating when deposition (Zhuhai Formation) recommenced. Might be resulted from the joint effect of the convergence of the Philippine Sea Plate to the Eurasian Plate and slab-pull force due to subduction of the SCS slab along the Manila trench (Fig. 8b), another tectonic reactivation (Dongsha Event) took place in Late Miocene (Zhao SJ et al., 2012; Wu SG et al., 2014), accompanied with faulting, erosion, igneous activity and hydrothermal fluid flow (Yan P et al., 2001). Samples were subjected to cooling again in response to this event, reheating commenced afterward due to sediments deposition since about 9 Ma (Fig. 8a).

6.2. A rough estimation of the erosion thickness and rate

The modeled t-T paths indicate three phases of cooling since the Middle Eocene, which occurred approximately in the Late Eocene (about 41 Ma), Early Oligocene (about 32

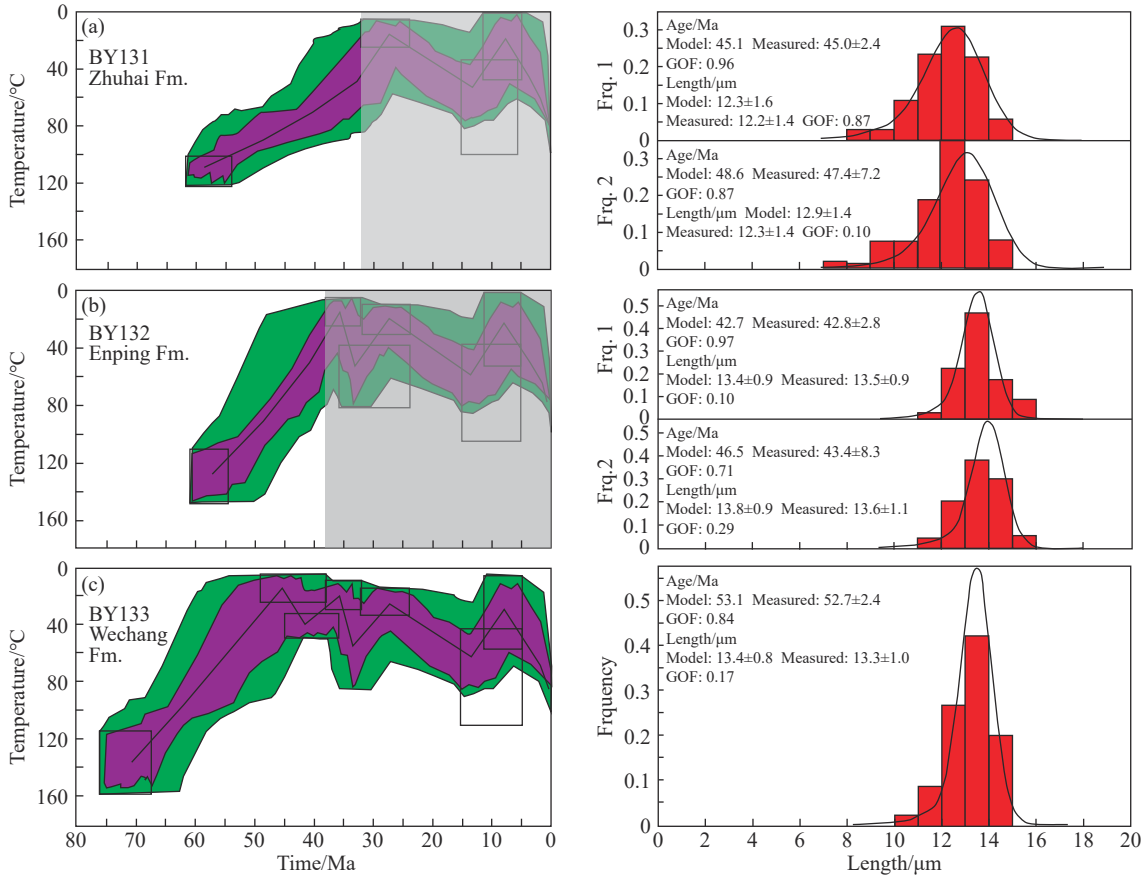

Fig. 5. Thermal history results for Well BY13 in the Pearl River Mouth Basin, from simultaneously modeling of samples from (a) Zhuhai Formation (BY131), (b) Enping Formation (BY132), and (c) Wenchang Formation (BY133) (HeFTy version 1.9.3, Ketcham RA et al., 2018). Data are provided in Tables 2 and 3. Displayed are the time-Temperature (t-T) paths (left), the c-axis corrected confined fission-track length-frequency distribution overlain by a calculated probability density function (best fit) (except for sample BY131, see text section 5.1 for further details). Green and pink envelopes indicate the realm of time-temperature solutions for acceptable (goodness-of-fit (GOF) > 0.05) and good (GOF > 0.5) paths, respectively. Blue lines are the weighted mean paths generated by averaging all successful paths as each nodal position). Shaded areas are regions of t-T space that are controlled by the sample below, while non-shaded areas are independent. Boxes on t-T graphs are constraints through which t-T histories were forced to pass.

Ma), and Late Miocene (about 13 Ma).

Assuming all the cooling was the consequence of erosion, the corresponding thickness and rate were calculated and presented in detail in Table 4. In Well BY13, erosion thickness is about 455 m, 747 m, and 800 m, with the erosion rate of about 0.08 mm/a, 0.13 mm/a, and 0.14 mm/a during the three cooling stages. In well HF28, the erosion thickness is about 712 m, 814 m, and 3419 m, with the erosion rate of about 0.12 mm/a, 0.21 mm/a, and 1.21 mm/a during three cooling stages. In the Well XJ24, only that sample from the Zhuhai Formation can be used to model thus only unravel the last cooling event, with erosion thickness of about 2849 m and the erosion rate of about 0.91 mm/a. Compared with the first two stages of erosion, the erosion thickness of the third stage for well HF28 and Well XJ24 seems to be too large and geological impossible. Thus, the third stage of cooling may not be simply ascribed to erosion.

As discussed in section 6.1, the third stage of cooling is likely to be caused by the Dongsha Movement, which was characterized by erosion, faulting, and magmatism (Wu SG et al., 2014). The spatial extent of the Dongsha Event is unclear. Some authors interpreted that the Dongsha Uplift and Chaoshan Depression are the prominently affected areas (Lüdmann T and Wong HK, 1999; Lüdmann T et al., 2001; Xia SH et al., 2017). While others argued that the post-rifting event also influenced the eastern part of the Panyu Low-uplift and the southern and northeastern parts of the Zhu I Depression (Huang CY et al., 2001; Wu SG et al., 2014) and an even larger area, for example, the Taiwan shelf (Lin CS et al., 2006). Since Well HF28 and XJ24 are near the Dongsha Uplift (Fig. 1), the phase of rapid cooling might primarily reflect geothermal readjustment after the cessation of the magmatism-related hydrothermal system, with the combined effect of erosion and faulting. As a result, we are unable to resolve the exhumation and erosion rate inferred from the cooling rate determined. To be noticed, although thickness (800 m) and rate (0.14 mm/a) related to the third cooling stage in Well BY 13 seems quite reasonable caused by erosion (Table 4), the magmatism and faulting effect of the Dongsha Event cannot be excluded.

6.3. Heating and hydrocarbon potential

In the PRMB, high-quality petroleum source rocks were

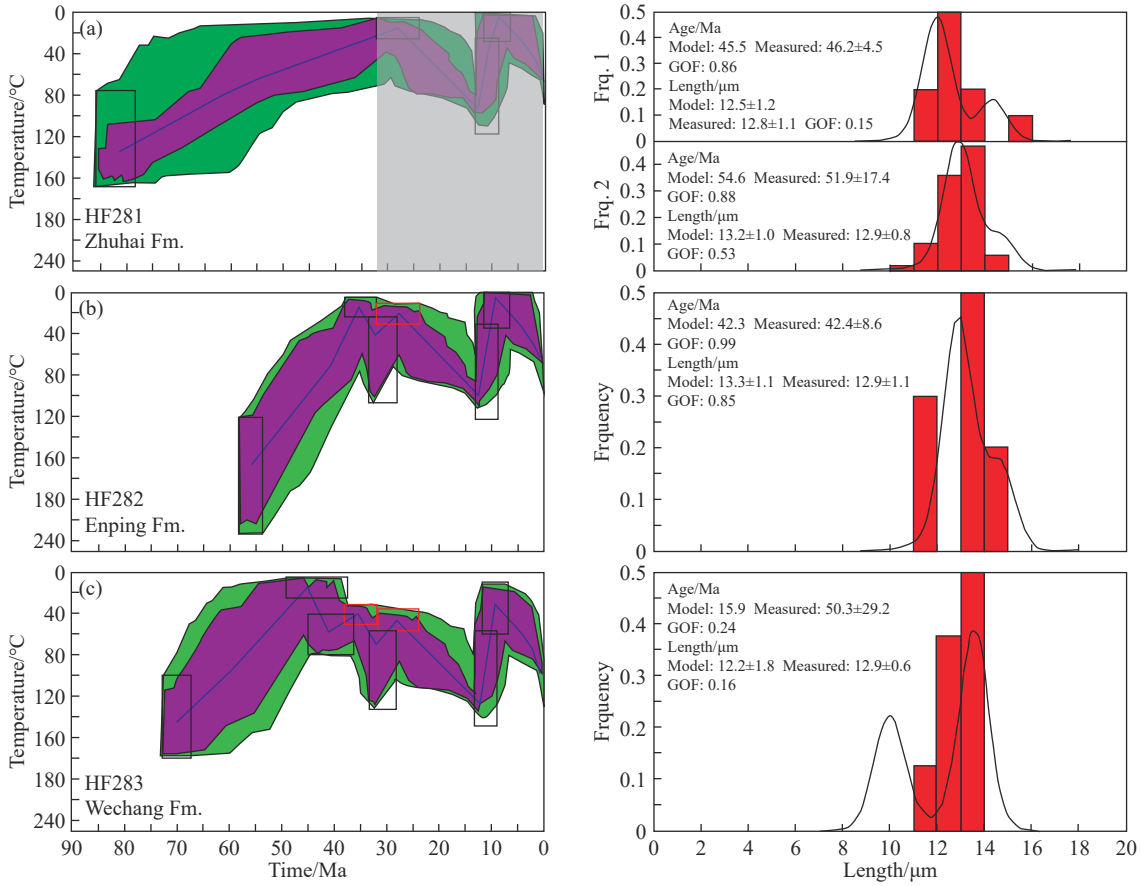

Fig. 6. Thermal history results for Well HF28 in the Pearl River Mouth Basin, from simultaneously modeling of samples from (a) Zhuhai Formation (HF281), (b) Enping Formation (HF282), and (c) Wenchang Formation (HF283).

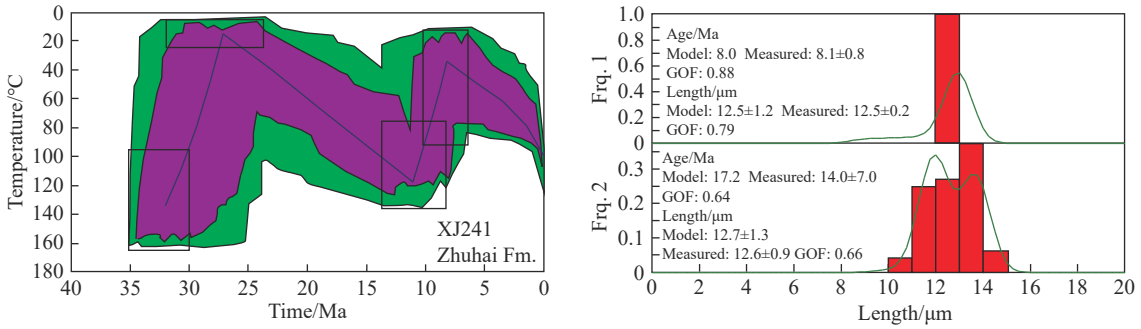

Fig. 7. Thermal histories of sample XJ241 from the Zhuhai Formation in Well XJ24, Pearl River Mouth Basin.

found in Wenchang and Enping Formations, with average TOC of 2.23% and 1.78%, respectively (Zhang SC et al., 2003). Vitrinite reflectance (Ro) measurements point out early to the middle mature organic matter in the Wenchang Formation (%R_o of 0.54–0.93) and early to the late mature organic matter in the Enping Formation (%R_o of 0.55–1.54) (Zhu JZ et al., 2007). In well BY13, the Wenchang and Enping Formations are currently exposed to the highest paleotemperature with a value of 94°C and 89°C. In well HF28, the source rocks in the Wenchang and Enping Formations underwent the highest palaeotemperature at the value of 128°C and 101 °C. Since most oil generation occurs at temperatures between 50°C and 150°C and most methane is generated between temperatures of 100°C and 225°C (Pashin JC, 2014), thermochronological data confirm that source rocks from Wenchang and Enping Formations in the PRMB have been exposed to the temperature necessary for oil and gas generation.

7. Conclusions

On basis of the new AFT dataset and thermal history modeling results, we draw the following conclusions.

(i) Thermal history reconstructed from both multiple-sample and single-sample modeling suggested that the Pearl River Mouth Basin has experienced four stages of heating separated by three phases of cooling since the Middle Eocene.

(ii) The first and second cooling events are likely to be erosion-driven; showing a strong correlation with unconformity related to the Zhuqiong II Event and Nanhai

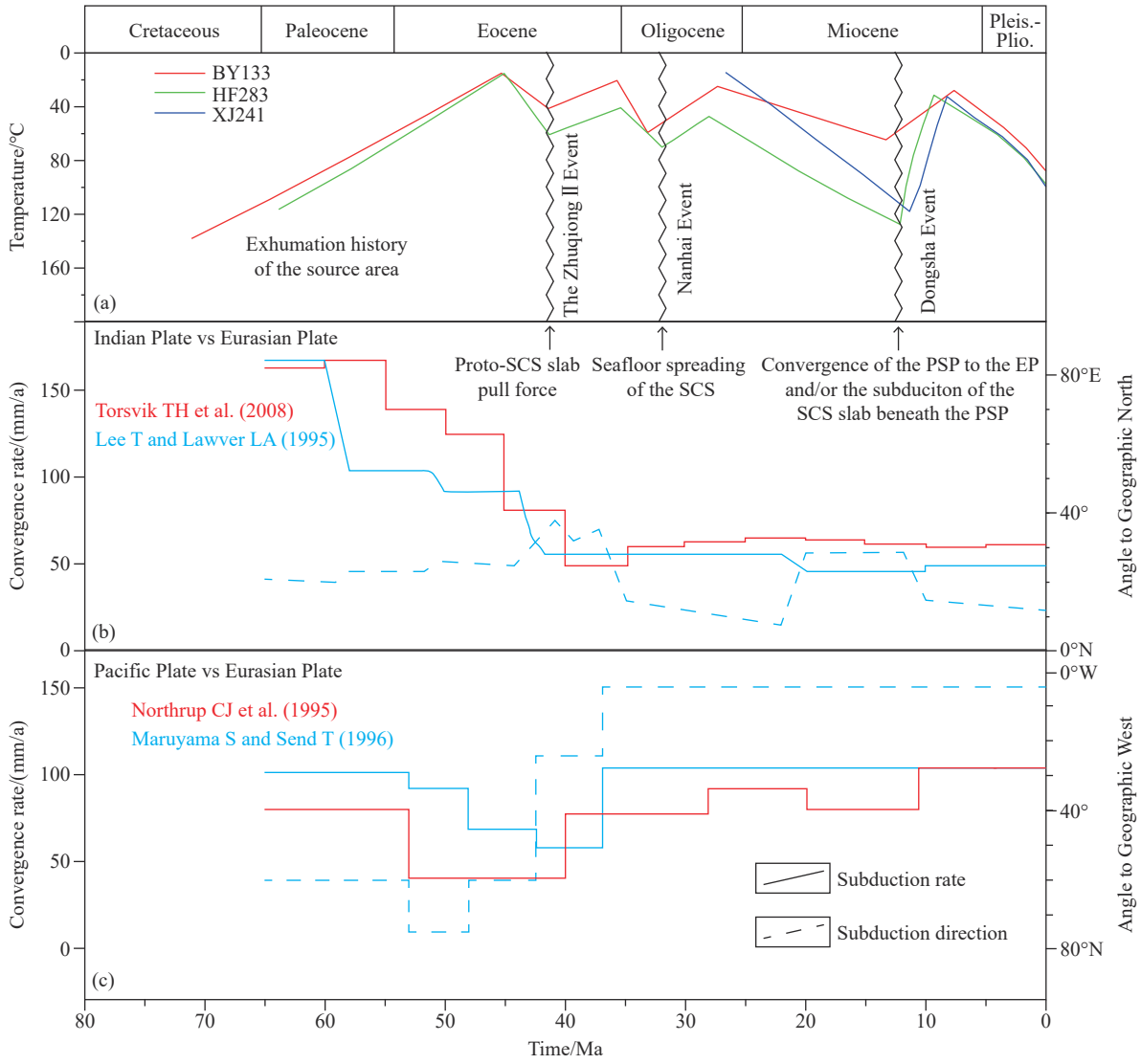

Fig. 8. (a) Weighted mean time-temperature paths for sample BY133, HF283, and XJ241, (b) Convergence rates and direction between the Indian–Eurasian Plates (Lee T and Lawver LA, 1995; Torsvik TH et al., 2008), and (c) Convergence rates and direction between the Pacific–Eurasian Plates (Maruyama S and Send T, 1986; Northrup CJ et al., 1995).

Table 4. Erosion thickness and rate estimation for three wells in the Pearl River Mouth Basin.

Sample	Time segment/Ma	Temperature segment/°C	Erosion thickness/m	Erosion Rate/(mm/a)
BY133	41-36	41-21	455	0.08
	33-27	59-25	747	0.13
	13-8	65-28	800[a]	0.14[a]
HF283	41-35	61-41	712	0.12
	32-28	70-47	814	0.21
	12-9	128-31	3419[a]	1.21[a]
XJ241	11-8	118-32	2849[a]	0.91[a]

Erosion rates were calculated considering heating and cooling rates, seafloor temperature, and geothermal gradient (see Table 1). [a] is speculative, see section 6.2 in the manuscript for further explanation.

Event, respectively. The erosion amount attributed to the first two cooling events is a range of a few hundred meters. The third cooling is likely the integrated consequence of erosion combined with magmatic activities coeval with the Dongsha Event, the erosion amount is thus difficult to decipher.

(iii) Time-temperature paths indicate heating up to 89°C–94°C of the Zhuhai samples and 101°C–128°C of the Wenchang samples during geologic time, confirming the necessary temperature for hydrocarbon generation of the source rocks.

CRediT authorship contribution statement

Xiao-yin Tang and Shu-chun Yang conceived of the presented idea. Sheng-biao Hu verified the analytical methods and supervised the findings of this work. All authors discussed the results and contributed to the final manuscript.

Declaration of Competing Interest

The authors declare no conflicts of interest.

Acknowledgment

This study is financially supported by the National Natural Science Foundation of China (42072181). We thank

Raymond Donelick and Paul O'Sullivan from the A to Z Inc. for the sample analysis.

Supplementary Material

Supplementary data (Figs. S1–S3; Tables. S1–S12) to this article can be found online at doi: 10.31035/cg2022055

Fig. S1. Length distribution of apatite confined fission tracks of samples from the Pearl River Mouth Basin. Lm = measured mean confined track length (±σ) (μm), N = number of tracks.

Fig. S2. Confined track lengths VS Dpar of each sample.

Fig. S3. Results of single-grain apatite fission-track ages (1σ) and Dpar of each sample.

Tables. S1-S12. Summary of Apatite fission-track age and confined track length data for all the 12 samples from the Pearl River Mouth Basin.

References

Carminati E, Cavazza D, Scrocca D, Fantoni R, Scotti P, Doglioni C. 2010. Thermal and tectonic evolution of the southern Alps (northern Italy) rifting: Coupled organic matter maturity analysis and thermokinematic modeling. AAPG Bulletin, 94(3), 369–397. doi: 10.1306/08240909069.

Clift P, Lin J. 2001. Preferential mantle lithospheric extension under the South China margin. Marine and Petroleum Geology, 18(8), 929–945. doi: 10.1016/S0264-8172(01)00037-X.

Donelick RA, O'Sullivan PB, Ketcham RA. 2005. Apatite fission-track analysis. Reviews in Mineralogy and Geochemistry, 58(1), 49–94. doi: 10.2138/rmg.2005.58.3.

Dong DD, Wu SG, Zhang GG, Yuan SQ. 2008. Rifting process and formation mechanisms of syn-rift stage prolongation in the deepwater basin, northern South China Sea. Chinese Science Bulletin, 53(23), 3715–3725. doi: 10.1360/csb2008-53-19-2342.

Dong DD, Zhang GC, Zhong K, Yuan SQ, Wu SG. 2009. Tectonic Evolution and Dynamics of Deepwater Area of Pearl River Mouth Basin, Northern South China Sea. Journal of Earth Science, 20(1), 147–159. doi: 10.1007/s12583-009-0016-1.

Galbraith RF. 1990. The radial plot: graphical assessment of spread in ages. International Journal of Radiation Applications and Instrumentation. Part D. Nuclear Tracks and Radiation Measurements, 17(3), 207–214. doi: 10.1016/1359-0189(90)90036-W.

Gallagher K. 1995. Evolving temperature histories from apatite fission-track data. Earth and Planetary Science Letters, 136(3–4), 421–435. doi: 10.1016/0012-821X(95)00197-K.

Gallagher K, Brown R, Johnson C. 1998. Fission track analysis and its applications to geological problems. Annual Review of Earth and Planetary Sciences, 26, 519–572. doi: 10.1146/annurev.earth.26.1.519.

Gleadow A, Duddy IR, Green PF, Hegarty KA. 1986. Fission track lengths in the apatite annealing zone and the interpretation of mixed ages. Earth and Planetary Science Letters, 78(2–3), 245–254. doi: 10.1016/0012-821X(86)90065-8.

He LJ, Wang KL, Xiong LP, Wang JY. 2001. Heat flow and thermal history of the South China Sea. Physics of the Earth and Planetary Interiors, 126(3–4), 211–220. doi: 10.1016/S0031-9201(01)00256-4.

Huang CY, Xia KY, Yuan PB, Chen PG. 2001. Structural evolution from Paleogene extension to Latest Miocene-Recent arc-continent collision offshore Taiwan: comparison with on land geology. Journal of Asian Earth Sciences, 19(5), 619–638. doi: 10.1016/s1367-9120(00)00065-1.

Jiang S, Zuo YH, Yang MH, Feng RP. 2021. Reconstruction of the Cenozoic tectono-thermal history of the Dongpu Depression, Bohai Bay Basin, China: Constraints from apatite fission track and vitrinite reflectance data. Journal of Petroleum Science and Engineering, 205, 108809. doi: 10.1016/j.petrol.2021.108809.

Jiang ZL, Zhu JZ, Deng HW, Hou DJ. 2012. Petroleum system and hydrocarbon accumulation characteristics in the wenchang and enping formations in the Huizhou Sag, Pearl River Mouth Basin, China. Energy Exploration and Exploitation, 30(3), 351–371. doi: 10.1260/0144-5987.30.3.351.

Ketcham RA. 2005. Forward and inverse modeling of low-temperature thermochronometry data. Reviews in Mineralogy and Geochemistry, 58, 275–314. doi: 10.2138/rmg.2005.58.11.

Ketcham RA, Mora A, Parra M. 2018. Deciphering exhumation and burial history with multi-sample down-well thermochronometric inverse modelling. Basin Research, 30(S1), 48–64. doi: 10.1111/bre.12207.

Kohn BP, Gleadow AJW, Brown RW, Gallagher K, Lorencak M, Noble WP. 2005. Visualizing thermotectonic and denudation histories using apatite fission track thermochronology. Reviews in Mineralogy and Geochemistry, 58(1), 527–565. doi: 10.2138/rmg.2005.58.20.

Lüdmann T, Wong HK. 1999. Neotectonic regime on the passive continental margin of the northern South China Sea. Tectonophysics, 311(1–4), 113–138. doi: 10.1016/S0040-1951(99)00155-9.

Lüdmann T, Wong HK, Wang P. 2001. Plio–Quaternary sedimentation processes and neotectonics of the northern continental margin of the South China Sea. Marine Geology, 172(3–4), 331–358. doi: 10.1016/S0025-3227(00)00129-8.

Lee T, Lawver LA. 1995. Cenozoic plate reconstruction of Southeast Asia. Tectonophysics, 251(1–4), 85–138. doi: 10.1016/0040-1951(95)00023-2.

Li ST, Lin CS, Zhang QM, Yang SG, Wu PK. 1999. Episodic rifting of continental marginal basins and tectonic events since 10 Ma in the South China Sea. Chinese Science Bulletin-English edition, 44(1), 10–23. doi: 10.1007/BF03182877.

Li YJ, Jiang ZL, Jiang S, Liu H, Wang BG. 2019. Heat flow and thermal evolution of a passive continental margin from shelf to slope – A case study on the Pearl River Mouth Basin, northern South China Sea. Journal of Asian Earth Sciences, 171, 88–102. doi: 10.1016/j.jseaes.2017.12.011.

Li XJ, Wang Z, Yao YJ, Gao HF, Zhu S, Xu ZY, 2022. Formation and evolution of the South China Sea since the Late Mesozoic: A review. China Geology. doi: 10.31035/cg2022021.

Lin CS, Gao JY, Yu XJ, Ye F, Tan YJ. 2006. Characteristics of tectonic movement in the northern part of South China Sea during the Cenozoic. Acta Oceanologica Sinica, 28(4), 81–86 (in Chinese with English abstract). doi: 10.3321/j.issn:0253-4193.2006.04.010.

Liu C, Clift PD, Carter A, Böning P, Hu Z, Sun Z, Pahnke K. 2017. Controls on modern erosion and the development of the Pearl River drainage in the late Paleogene. Marine Geology, 394, 52–68. doi: 10.1016/j.margeo.2017.07.011.

Maruyama S, Send T. 1986. Orogeny and relative plate motions: Example of the Japanese Islands. Tectonophysics, 127(3–4), 305–329. doi: 10.1016/0040-1951(86)90067-3.

Northrup CJ, Royden LH, Burchfiel BC. 1995. Motion of the Pacific plate relative to Eurasia and its potential relation to Cenozoic extension along the eastern margin of Eurasia. Geology, 23(8), 719–722. doi: 10.1130/0091-7613(1995)023<0719:MOTPPR>2.3.CO;2.

Pashin JC, 2014. Geology of North American coalbed methane reservoirs, Coal Bed Methane. Elsevier, 31–61. doi: 10.1016/B978-0-12-800880-5.00003-6.

Qiu NS, Chang J, Zuo YH, Wang JY, Li HL. 2012. Thermal evolution and maturation of lower Paleozoic source rocks in the Tarim Basin, northwest China. AAPG Bulletin, 96(5), 789–821. doi: 10.1306/09071111029.

Qiu NS, Zuo YH, Chang J, Li WZ. 2014. Geothermal evidence of Meso-Cenozoic lithosphere thinning in the Jiyang sub-basin, Bohai Bay Basin, eastern North China Craton. Gondwana Research, 26(3–4), 1079–1092. doi: 10.1016/j.gr.2013.08.011.

Rao CT, Li PL. 1991. Heat flow of Pearl River Mouth Basin. China Offshore Oil and Gas (Geology), 5(6), 7–18.

Ru K, Zhou D, Chen HZ, 1994. Basin evolution and hydrocarbon potential of the northern South China Sea. Netherlands, Kluwer Academic Publishers, 361–372.

Rudnick RL, McDonough WF, O'Connell RJ. 1998. Thermal structure, thickness and composition of continental lithosphere. Chemical Geology, 145(3–4), 395–411. doi: 10.1016/s0009-2541(97)00151-4.

Shao L, Cao LC, Pang X, Jiang T, Qiao PJ, Zhao M. 2016. Detrital zircon provenance of the Paleogene synrift sediments in the northern South China Sea. Geochemistry, Geophysics, Geosystems, 17(2), 255–269. doi: 10.1002/2015GC006113.

Shao L, Meng AH, Li QY, Qiao PJ, Cui YC, Cao LC, Chen SH. 2017. Detrital zircon ages and elemental characteristics of the Eocene sequence in IODP Hole U1435A: Implications for rifting and environmental changes before the opening of the South China Sea. Marine Geology, 394, 39–51. doi: 10.1016/j.margeo.2017.08.002.

Shi XB, Qiu XL, Xia KY, Zhou D. 2003. Characteristics of surface heat flow in the South China Sea. Journal of Asian Earth Sciences, 22(3), 265–277. doi: 10.1016/S1367-9120(03)00059-2.

Song Y, Zhao CY, Zhang GC, Song HB, Shan JN, Chen L. 2011. Research on tectono-thermal modeling for Qiongdongnan Basin and Pearl River Mouth Basin in the northern South China Sea. Chinese Journal of Geophysics, 54(12), 3057–3069 (in Chinese with English abstract). doi: 10.1002/cjg2.1675.

Tang XY, Hu SB, Zhang GC, Yang SC, Shen HL, Rao S, Li WW. 2014. Characteristic of surface heat flow in the Pearl River Mouth Basin and its relationship with thermal lithosphere thickness. Chinese Journal of Geophysics, 57(6), 1857–1867 (in Chinese with English abstract). doi: 10.6038/cjg20140617.

Tang XY, Huang SP, Yang SC, Jiang GZ, Hu SB. 2016. Correcting on Logging-derived temperatures of the Pearl River Mouth Basin and characteristics of its present temperature field. Chinese Journal of Geophysics, 59(8), 2911–2921 (in Chinese with English abstract). doi: 10.6038/cjg20160816.

Tang XY, Huang SP, Yang SC, Jiang GZ, Ji M, Hu SB. 2018a. Tectono-thermal evolution of the Liwan Sag, deepwater area in the Zhujiang River Mouth Basin, northern South China Sea. Acta Oceanologica Sinica, 37(2), 66–75. doi: 10.1007/s13131-017-1125-9.

Tang XY, Yang SC, Hu SB. 2018b. Thermal-history reconstruction of the Baiyun Sag in the deep-water area of the Pearl River Mouth Basin, northern South China Sea. Frontiers of Earth Science, 12(3), 532–544. doi: 10.1007/s11707-017-0675-7.

Tang XY, Yang SC, Zhu JZ, Long ZL, Jiang GZ, Huang SP, Hu SB. 2017. Tectonic subsidence of the Zhu 1 Sub-basin in the Pearl River Mouth Basin, northern South China Sea. Frontiers of Earth Science, 11(4), 729–739. doi: 10.1007/s11707-016-0610-3.

Tang XY, Zuo YH, Kohn B, Li Y, Huang SP. 2019. Cenozoic thermal history reconstruction of the Dongpu Sag, Bohai Bay Basin: insights from apatite fission-track thermochronology. Terra Nova, 31(3), 159–168. doi: 10.1111/ter.12379.

Tian ZH, Xiao WJ, Zhang ZY, Lin X. 2016. Fisson-track constrains on superposed folding in the Beishan orogenic belt, southernmost Altaids. Geoscience Frontiers, 7(2), 181–196. doi: 10.1016/j.gsf.2015.11.007.

Torsvik TH, Müller R, Rob V, Steinberger B, Gaina C. 2008. Global plate motion frames: Toward a unified model. Reviews of Geophysics, 46(RG3004). doi: 10.1029/2007RG000227.

Vermeesch P. 2009. RadialPlotter: A Java application for fission track, luminescence and other radial plots. Radiation Measurements, 44(4), 409–410. doi: 10.1016/j.radmeas.2009.05.003.

Wang PC, Li SZ, Suo YH, Guo LL, Santosh M, Li XY, Wang GZ, Jiang ZX, Liu B, Zhou J, Jiang SH, Cao XZ, Liu Z. 2021. Structural and kinematic analysis of Cenozoic rift basins in South China Sea: A synthesis. Earth-Science Reviews, 216(2), 103522. doi: 10.1016/j.earscirev.2021.103522.

Wang PC, Li SZ, Suo YH, Guo LL, Wang GZ, Hui GG, Santosh M, Somerville ID, Cao XZ, Li Y. 2020. Plate tectonic control on the formation and tectonic migration of Cenozoic basins in northern margin of the South China Sea. Geoscience Frontiers, 11(4), 1231–1251. doi: 10.1016/j.gsf.2019.10.009.

Wang W, Ye JR, Bidgoli T, Yang XH, Shi HS, Shu Y. 2017. Using detrital zircon geochronology to constrain Paleogene provenance and its relationship to rifting in the Zhu 1 Depression, Pearl River Mouth Basin, South China Sea. Geochemistry, Geophysics, Geosystems, 18(11), 3976–3999. doi: 10.1002/2017GC007110.

White N, Thompson M, Barwise T. 2003. Understanding the thermal evolution of deep-water continental margins. Nature, 426(6964), 334–343. doi: 10.1038/nature02133.

Wu SG, Gao JW, Zhao SJ, Lüdmann T, Chen DX, Spence G. 2014. Post-rift uplift and focused fluid flow in the passive margin of northern South China Sea. Tectonophysics, 615-616(1), 27–39. doi: 10.1016/j.tecto.2013.12.013.

Wu XJ, Pang X, Shi HS, He M, Shen J, Zhang XT, Hu DK. 2009. Deep structure and dynamics of passive continental margin from shelf to ocean of the northern South China Sea. Journal of Earth Science, 20(1), 38–48. doi: 10.1007/s12583-009-0004-5.

Xiang CF, Pang X, Danišík M. 2013. Post-Triassic thermal history of the Tazhong Uplift Zone in the Tarim Basin, Northwest China: Evidence from apatite fission-track thermochronology. Geoscience Frontiers, 4(6), 743–754. doi: 10.1016/j.gsf.2012.11.010.

Xia SH, Fan CY, Sun JL, Cao JH, Zhao F, Wan KY. 2017. Characteristics of late Cenozoic magmatic activities on the northern margin of South China Sea and their tectonic implications. Marine Geology & Quaternary Geology, 37(6), 25–33 (in Chinese with English abstract). doi: 10.16562/j.cnki.0256-1492.2017.06.003.

Xie H, Zhou D, Pang X, Li YP, Wu XJ, Qiu N, Li PC, Chen GH. 2013. Cenozoic sedimentary evolution of deepwater sags in the Pearl River Mouth Basin, northern South China Sea. Marine Geophysical Research, 34(3), 159–173. doi: 10.1007/s11001-013-9183-7.

Xie XN, Müller RD, Li ST, Gong ZS, Steinberger B. 2006. Origin of anomalous subsidence along the Northern South China Sea margin and its relationship to dynamic topography. Marine and Petroleum Geology, 23(7), 745–765. doi: 10.1016/j.marpetgeo.2006.03.004.

Yan P, Deng H, Liu HL, Zhang ZR, Jiang YK. 2006. The temporal and spatial distribution of volcanism in the South China Sea region. Journal of Asian Earth Sciences, 27(5), 647–659. doi: 10.1016/j.jseaes.2005.06.005.

Yan P, Zhou D, Liu ZS. 2001. A crustal structure profile across the northern continental margin of the South China Sea. Tectonophysics, 338(1), 1–21. doi: 10.1016/S0040-1951(01)00062-2.

Yan Y, Andy C, Bin X, Lin G, Stephanie B, Hu XQ. 2009. A fission-track and (U-Th)/He thermochronometric study of the northern margin of the South China Sea: An example of a complex passive margin. Tectonophysics, 474(3–4), 584–594. doi: 10.1016/j.tecto.2009.04.030.

Ye Q, Mei LF, Shi HS, Camanni G, Shu Y, Wu J, Yu L, Deng P, Li G. 2018. The Late Cretaceous tectonic evolution of the South China Sea area: An overview, and new perspectives from 3D seismic reflection data. Earth-Science Reviews, 187, 186–204. doi: 10.1016/j.earscirev.2018.09.013.

Yuan YS, Zhu WL, Mi LJ, Zhang GC, Hu SB, He LJ. 2009. “Uniform geothermal gradient” and heat flow in the Qiongdongnan and Pearl River Mouth Basins of the South China Sea. Marine and Petroleum

Geology, 26(7), 1152–1162. doi: 10.1016/j.marpetgeo.2008.08.008.

Zhang CM, Li ST, Yang JM, Yang SK, Wang H. 2004. Petroleum migration and mixing in the Pearl River Mouth Basin, South China Sea. Marine and Petroleum Geology, 21(2), 215–224. doi: 10.1016/j.marpetgeo.2003.11.010.

Zhang SC, Liang DG, Gong ZS, Wu KQ, Li MW, Song FQ, Song ZG, Zhang DJ, Wang PR. 2003. Geochemistry of petroleum systems in the eastern Pearl River Mouth Basin: evidence for mixed oils. Organic Geochemistry, 34(7), 971–991. doi: 10.1016/S0146-6380(03)00034-2.

Zhang ZY, Zhu WB, Zheng DW, Zheng BH, Yang W. 2016. Apatite fission track thermochronology in the Kuluketage and Aksu areas, NW China: Implication for tectonic evolution of the northern Tarim. Geoscience Frontiers, 7(2), 171–180. doi: 10.1016/j.gsf.2015.08.007.

Zhao SJ, Wu SG, Shi HS, Dong DD, Chen DX, Wang Y. 2012. Structures and dynamic mechanism related to the Dongsha movement at the northern margin of South China Sea. Progress in Geophysics, 27(3), 1008–1019 (in Chinese with English abstract). doi: 10.6038/j.issn.1004-2903.2012.03.022.

Zhou D, Ru K, Chen HZ. 1995. Kinematics of Cenozoic extension on the South China Sea continental margin and its implications for the tectonic evolution of the region. Tectonophysics, 251(1–4), 161–177. doi: 10.1016/0040-1951(95)00018-6.

Zhu JZ, Shi HS, Shu Y, Du JY, Wu JY, Luo JL. 2007. Organic maceral characteristics and hydrocarbon-generating potentials of source rocks in the Pearl River Mouth Basin. Petroleum Geology and Experiment, 29(3), 301–306 (in Chinese with English abstract). doi: 10.3969/j.issn.1001-6112.2007.03.015.

Zhu WL, Li MB, Wu PK. 1999. Petroleum systems of the Zhu III subbasin, Pearl River Mouth Basin, South China Sea. AAPG Bulletin, 83(6), 990–1003. doi: 10.1306/e4fd2e47-1732-11d7-8645000102c1865d.

Zhu WL, Zhong K, Li YC, Xu Q, Fang DY. 2012. Characteristics of hydrocarbon accumulation and exploration potential of the northern South China Sea deepwater basins. Chinese Science Bulletin-English edition, 57(24), 3121–3129. doi: 10.1007/s11434-011-4940-y.

Zhu WL, Huang BJ, Mi LJ, Wilkins RWT, Fu N, Xiao XM. 2009. Geochemistry, origin, and deep-water exploration potential of natural gases in the Pearl River Mouth and Qiongdongnan basins, South China Sea. AAPG Bulletin, 93(6), 741–761. doi: 10.1306/02170908099.

Zuo YH, Ye B, Wu WT, Zhang YX, Ma WX, Tang SL, Zhou YS. 2017. Present temperature field and Cenozoic thermal history in the Dongpu depression, Bohai Bay Basin, North China. Marine and Petroleum Geology, 88(Supplement C), 696–711. doi: 10.1016/j.marpetgeo.2017.08.037.